Research Article

*For reprint orders, please contact: reprints@futuremedicine.com*

Nanomedicine

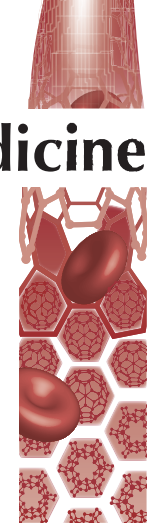

# Clustering superparamagnetic iron oxide nanoparticles produces organ-targeted high-contrast magnetic resonance images

Nicholas J Hobson[1,2], Xian Weng[1,2], Bernard Siow[3], Catarina Veiga[4], Marianne Ashford[5], Nguyen TK Thanh[2,6], Andreas G Schätzlein[1] & Ijeoma F Uchegbu*[,1]

[1]UCL School of Pharmacy, 29–39 Brunswick Square, WC1N 1AX London

[2]UCL Healthcare Biomagnetic & Nanomaterials Laboratories, 21 Albemarle Street, W1S 4BS London

[3]Centre for Advanced Biomedical Imaging, UCL, Gower Street, WC1E 6BT London

[4]UCL Medical Physics & Biomedical Engineering, Malet Place, Gower Street, WC1E 6BT London

[5]Advanced Drug Delivery, Pharmaceutical Sciences, IMED Biotech Unit, AstraZeneca, Macclesfield, SK10 2NA Cheshire

[6]Biophysics Group, UCL, Gower Street, WC1E 6BT London

*Author for correspondence: ijeoma.uchegbu@ucl.ac.uk

**Aim:** Superparamagnetic iron oxide nanoparticles (SPIONs) have been used as magnetic resonance imaging (MRI) contrast agents; however, a number of T2-weighted imaging SPIONs have been withdrawn due to their poor clinical contrast performance. Our aim was to significantly improve SPION T2-weighted MRI contrast by clustering SPIONs within novel chitosan amphiphiles. **Methods:** Clustering SPIONs was achieved by encapsulation of hydrophobic-coated SPIONs with an amphiphilic chitosan polymer (GCPQ). **Results:** Clustering increases the spin-spin ($r_2$) to spin-lattice ($r_1$) relaxation ratio ($r_2/r_1$) from 3.0 to 79.1, resulting in superior contrast. Intravenously administered clustered SPIONs accumulated only in the liver and spleen; with the reduction in T2 relaxation confined, in the liver, to the extravascular space, giving clear MRI images of the liver vasculature.

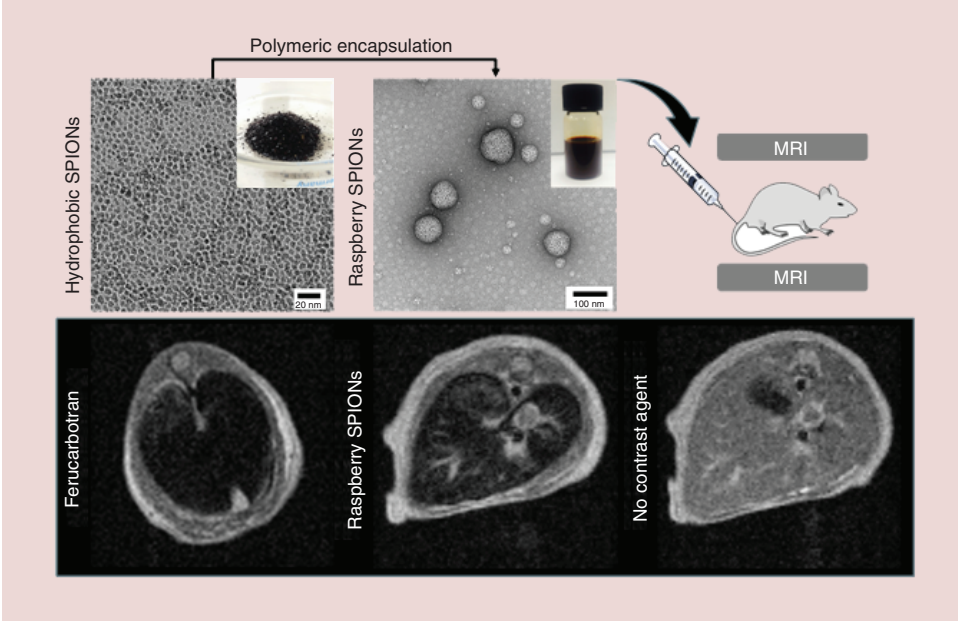


First draft submitted: 2 October 2018; Accepted for publication: 28 January 2019; Published online: 3 May 2019

**Keywords:** chitosan amphiphile • GCPQ • micelle • MRI contrast agent • SPIONs • superparamagnetic iron oxide nanoparticles

Future Medicine

In the future, it is predicted that medicine will rely heavily on more accurate diagnosis of patients, especially as medicines become more personalized [1,2]. Magnetic resonance imaging (MRI) is a powerful diagnostic technique that is able to give excellent anatomical images in a noninvasive real-time manner using nonionizing radiation [3]. This said, however, it can often be challenging to distinguish between healthy and diseased sites in the same tissue and so contrast agents are routinely employed to enhance the sensitivity of the technique [4]. Over the last three decades, superparamagnetic iron oxide nanoparticles (SPIONs) have gained considerable attention as negative MRI contrast agents due to their unique magnetic properties [5–9]. In recent years however, a number of prominent SPION contrast agents have been withdrawn or discontinued [10–13]. While it is difficult to ascertain the precise reasons for the withdrawal, clinical uptake was obviously a factor due presumably to the poor contrast obtained with these agents, when compared with gadolinium-based agents [14]. However, there are still considerable toxicity concerns associated with the use of gadolinium contrast agents, such as brain and bone accumulation and kidney toxicity [15], a fact that underpins the requirement for safer contrast agents. Our aim is to use nanoparticle engineering to prepare contrast agents from biocompatible materials, such as SPIONs, that produce unequivocal contrast images. We have discovered that clustering SPIONs into raspberry shapes within a polymeric envelope leads to vastly improved image contrast and it is the improved image contrast that is the thrust of the current work. The self-assembling polymer used is a chitosan amphiphile: N-palmitoyl-N-monomethyl-N-N-dimethyl-N-N-N-trimethyl-6-O-glycolchitosan (GCPQ), which has previously been used to deliver challenging drug molecules [16–19]. GCPQ has been through good laboratory practice standard preclinical toxicology testing with no toxicity issues observed and has shown good cell biocompatibility ($IC_{50}$ ~1 mg $ml^{-1}$) [20,21]. Previous studies attempting to encapsulate SPIONs within self-assembling aggregates have often yielded impressive *in vitro* results but many have limited or no information regarding their *in vivo* biological stability and/or their pharmacokinetic and pharmacodynamic characteristics [22–29]. *In vivo* evaluations are often challenging as polymeric surfactant nanoparticles are destabilized by biological environments where there is the presence of salts and proteins. Protein adsorption *in vivo* is a possible destabilizing factor. The work presented here clearly demonstrates that a positively charged raspberry SPION, comprising 5 nm SPIONs clustered into a larger raspberry shape, may be used as a superior MRI negative contrast agent. Clustering, as opposed to the synthesis of larger SPIONs, means that these 4–5 nm core size SPIONs are more likely to be excreted via the urine [30,31].

## Materials & methods

All chemicals and reagents were purchased from Sigma-Aldrich, UK unless otherwise specified. Dialysis membranes were purchased from Medicell International Ltd., London UK. All reagents were used without further purification. Animals were purchased from Harlan, UK.

### Synthesis of modified chitosan amphiphilic polymer: *N*-palmitoyl-*N*-monomethyl-*N,N*-dimethyl-*N,N,N*-trimethyl-6-O-glycolchitosan (GCPQ)

GCPQ was synthesized as described previously [18]. Briefly, glycol chitosan (5 g, molecular weight ~250 kDa, Wako Chemicals, Japan) was dissolved in 4M HCl (380 ml). The solution was heated to 50°C and stirred for 24 h. The resulting solution was dialyzed exhaustively against water (MWCO: 3.5 kDa) and then lyophilized to obtain a white fibrous solid. Yield = 46%, $M_w$ = 7 kDa, as measured by GPC-MALLS [32].

Degraded glycol chitosan (1.0 g) and $NaHCO_3$ (0.75 g) were dissolved into a mixture of ethanol and water (24:76). Palmitic acid *N*-hydroxysuccinimide (1.58 g, Toronto Research Chemicals, Canada) was dissolved into ethanol (300 ml) and was added drop wise. The reaction was left to stir for 72 h protected from light. Ethanol was removed under vacuum and the remaining aqueous phase extracted using diethyl ether three-times. The aqueous phase was dialyzed exhaustively against water (MWCO: 3.5 kDa) and then lyophilized to obtain a white fibrous solid. Yield = 96%.

Palmitoylated glycol chitosan chitosan (300 mg) was dispersed in *N*-methyl-2-pyrrolidone (25 ml) and stirred vigorously overnight. Sodium hydroxide (40 mg) dissolved in ethanol (2 ml) and sodium iodide (45 mg) dissolved in ethanol (2 ml) were both added to the solution and the reaction was heated to 36°C. Methyl iodide (0.45 ml) was added and the reaction was stirred under a nitrogen environment for 3 h. The product was precipitated using diethyl ether and left overnight. The resulting precipitate was washed three-times with diethyl ether (50 ml), dissolved in water (100 ml) and then dialyzed exhaustively against water (MWCO: 3.5 kDa). The dialysate was passed through an Amberlite IRA-96 column to remove iodide and lyophilized to obtain a white fibrous solid. Yield = 70%.

### Synthesis of iron oxide nanoparticles via high temperature decomposition

Iron oxide nanoparticles were synthesized in a procedure outlined by Kim *et al.* [33]. In a typical reaction, $FeCl_3.6H_2O$ (3.0 g) and sodium oleate (10.2 g, TCI Chemicals, Japan) were dissolved in a solvent mixture comprising: 17 ml water, 23 ml ethanol and 40 ml hexane. The resulting mixture was stirred for 4 h at 70°C. After 4 h, the reaction mixture was allowed to cool to room temperature and the hexane layer extracted and washed three-times with distilled water (30 ml). The hexane was then evaporated under vacuum to yield a waxy orange oil.

The iron–oleate complex (1.8 g) from above, oleic acid (0.57 g, CRODA, UK) and oleyl alcohol (1.61 g) were dissolved in diphenyl ether (10 g). The reaction mixture was heated to 250°C and then kept at this temperature for 20 min under a nitrogen atmosphere. The mixture was then rapidly cooled to room temperature and acetone (50 ml) was added to precipitate out the nanoparticles. Nanoparticles were collected via centrifugation (3000 rcf, 10 min) and the supernatant was discarded and replaced with acetone (40 ml) to wash the nanoparticles. The acetone was removed by centrifugation and the acetone wash was repeated three-times. The washed nanoparticles were finally dispersed and stored in hexane. To obtain dry nanoparticles for characterization, the hexane was removed under vacuum. Acetone was added and the nanoparticles gently collected with a spatula and dried overnight under vacuum. The particles were then weighed and made up to the desired concentration in hexane, chloroform or THF.

### Formulation raspberry SPIONs

In a small vial, iron oxide nanoparticles in hexane (2 ml, 4 mg/ml) were added to a GCPQ dispersion (5 ml, 1 mg/ml). The dispersion was then sonicated using probe sonication (2 × 5 min, Soniprep 150, MSE, UK) at the interface between the organic and aqueous phases, creating a brown emulsion. This emulsion was left to separate over 48 h. The aqueous layer was collected and any residual hexane was allowed to evaporate overnight. The product – raspberry SPIONs – was frozen and lyophilized to obtain a dry product, which rapidly dispersed when added to water (5 ml). For the *in vivo* investigations, a formulation with a higher level of iron oxide nanoparticles was made by increasing the SPIONs and polymer concentration by a factor of 15: iron oxide nanoparticles in hexane (2 ml, 60 mg/ml) were added to a GCPQ dispersion (5 ml, 15 mg/ml) and processed as described above.

### Fourier-transform infra-red spectroscopy

Fourier-transform infra-red (FT-IR) spectra were obtained using a PerkinElmer Spectrum 100 FT-IR Spectrometer equipped with a Universal attenuated total reflectance (ATR) accessory (PerkinElmer Inc., MA, USA). The sample was mounted onto the Universal diamond ATR top-plate and the force gauge was increased to 100 N. The spectrum was recorded in a range of 4000–650 $cm^{-1}$ using PerkinElmer Spectrum Express Version 1.02.00 software.

### Thermogravimetric analysis

Thermogravimetric analysis (TGA) measurements (Pyris 6 TGA; PerkinElmer Inc.) were performed on samples. Samples (5–6 mg) were weighed into a ceramic crucible. Nitrogen (20 ml $min^{-1}$) was used as a purge gas. The samples were heated from 20 to 450°C at 10°C $min^{-1}$. The mass loss between 20 and 100°C was used to determine the water content of samples. The onset of degradation was obtained using the Pyris Software for Windows Version 3.81 (PerkinElmer Instruments; PerkinElmer Inc.)

### Ligand exchange of iron oxide nanoparticles with *meso*-2,3-dimercaptosuccinic acid

This ligand exchange protocol was carried out according to the method previously described by Palma *et al.* [34]. Briefly, iron oxide nanoparticles (20 mg) were precipitated from the hexane disperse phase (1 ml) by the addition of ethanol and were collected via centrifugation (9000 rcf, 10 min). The supernatant was discarded and replaced with ethanol and this procedure was repeated twice. The final precipitate was re-dispersed in toluene. Dimercaptosuccinic acid (DMSA) (36 mg) in DMSO (2 ml) was added to the toluene mixture and the reaction was bath sonicated (10 min) and left to stir at room temperature for 48 h. After 48 h, a sediment was observed and this was collected via centrifugation (9000 rcf, 10 min). The supernatant was discarded and replaced with ethanol and this procedure was repeated twice. The final precipitate was re-dispersed in water, titrated to pH 10 using NaOH and then filtered through a 0.22 µm membrane.

### Transmission electron microscopy

Images were collected using an FEI CM120 BioTwin Transmission Electron Microscope (Ex. Philips, Eindhoven, The Netherlands). Digital images were captured using an AMT digital camera. A drop of the sample was placed

on Formvar©/Carbon Coated Grid (F196/100 3.05 mm, mesh 300, TAAB Labs Ltd, UK). Samples were stained with uranyl acetate (1%) where indicated.

### Dynamic light scattering

Particle size was determined by dynamic light scattering (DLS) on a Malvern Zetasizer Nano ZS (Malvern Instruments, UK) using a laser wavelength of 633 nm. Samples were inverted several times and then left to equilibrate for 10 s before particle sizing was carried out. The accuracy of the instrument was assessed periodically using latex beads (polystyrene, mean size: 0.1 μm) in 50 mM sodium chloride dispersant phase.

### Zeta potential & size measurements

The particles' zeta potentials were measured using a Malvern Zetasizer Nano ZS (Malvern Instruments) paired with an MPT-2 automatic titrator (Malvern Instruments). Prior to any titration, the pH probes were calibrated using pH 4, pH 7 and pH 10 standards. Nanoparticles were manually titrated to pH 4. The instrument then automatically titrated the sample and measured the particle size and zeta potential between pH 4 and 11. Reservoirs were filled with HCl and NaOH at concentrations of 0.05 M. Measurements were carried out in gold-plated disposable capillary cells (Malvern Instruments). The accuracy of the instrument was assessed periodically using a polystyrene zeta standard (Malvern Instruments).

### X-ray diffraction

X-ray diffraction patterns were collected on an x-ray diffractometer (PanAlytical, UK) using CoKα radiation λ = 1.79 Å. Samples were prepared by pressing dried powders on a zero background silicon wafer and diffraction patterns were collected within a 20–100 2θ (degrees) range.

### Magnetic properties

Magnetization curves were recorded in a Quantum Design hybrid Superconducting Quantum Interference Device-Vibrating Sample Magnetometer (SQUID-VSM) at 300 K, with applied fields up to 7 T. Samples were lyophilized to obtain a dry product. Weighed samples of the dry product were placed into plastic capsules and measured in a straw sample holder.

### Stability studies on raspberry SPIONs

The stability of the raspberry SPIONs was investigated in: $H_2O$, 0.9%w/v NaCl, phosphate-buffered saline ([PBS], pH = 7.4) and 5%w/v dextrose. Raspberry SPIONs were frozen and lyophilized to obtain a dry product and then dispersed in MilliQ water. Following this, the raspberry SPIONs (2.5 ml) were added to: $H_2O$ (2.5 ml), 1.8% NaCl (2.5 ml), double strength PBS (2.5 ml), 10%w/v dextrose (2.5 ml), diluting each of the buffers by a factor of 2 and were incubated at 37°C. At various time points aliquots were removed, centrifuged (224 rcf × 10 min) and then the supernatant was analyzed for iron content via the 1,10-phenanthroline iron quantification assay. Briefly, the supernatant (200 μl) was added to HCl (4M, 200 μl) and digested at 70°C. In a sample vial, sodium acetate (125 mg/ml, 450 μl) and hydroxylamine hydrochloride (10 mg/ml, 50 μl) were added to the supernatant (200 μl) followed by the 1,10-phenanthroline (10 mg/ml, 300 μl) turning the sample bright red if iron was present. Sample vials were stored, protected from light for 1 h and then measured using UV/VIS (ELx808 microplate reader, BioTek Instruments, UK) at 510 nm. The iron concentrations were determined based on a calibration curve made from iron(II) chloride tetrahydrate.

The plasma stability of the raspberry SPIONs was measured by measuring iron content of the colloidal fraction, using ICP-AES (Varian 720, Agilent, UK), after incubation in plasma. Blood was obtained from male Wistar rats (400–450 g, Harlan), collected into microtainer tubes coated in ethylene diamine tetraacetic acid (EDTA, K3E Vacutainer, BD Biosciences, UK) and maintained on ice. Plasma was obtained as the supernatant after centrifugation of blood samples (252 rcf × 10 min, 4°C) and stored at -20°C until required for the experiments. Raspberry SPIONs (0.5 mg/ml Fe, 2.5 ml) were added to rat plasma (2.5 ml), diluting the plasma by a factor of 2 and were incubated at 37°C. At various time points, aliquots were removed, centrifuged (224 rcf, 10 min) and the supernatant was analyzed for iron content using ICP-AES. Briefly, the supernatant (300 μl) was added to 70% $HNO_3$ (300 μl) and the particles digested at 70°C. The digestant was diluted by a factor of 35 with MilliQ water and the diluted sample was measured using ICP-AES. The iron concentrations were determined based on a calibration curve made from an iron standard for ICP-AES (TraceCERT, Fluka, UK).

### MRI contrast measurements

MR relaxivities were measured using a 1T bench-top MRI scanner (ICON™, Bruker, UK) at 37°C. For $r_2$ relaxation, a spin echo sequence was used with the following parameters: TE = 6–100 ms, TR = 1845 ms. The $r_2$ relaxivities were determined by curve fitting the echo times (TE) using MATLAB (Mathworks, UK). The relaxivities were plotted against the iron concentration and the $r_2$ determined from the gradient of the slope. $r_1$ relaxivity was measured using an inversion recovery sequence with the following parameters: TI = 35–7500 ms, TR = 15000. The $r_1$ relaxivities were determined by curve fitting several inversion times (TI). The relaxivities were plotted against concentration and $r_1$ determined from the gradient of the slope.

### Biodistribution studies

Female BALB/c mice were used (20–25 g, Harlan). All animal experiments were performed under a UK Home Office Animal License and in accordance with local ethics committee rules. A raspberry SPION suspension (6.5 mg Fe/ml) was prepared in 5% dextrose, titrated to pH 6 using 0.1 M NaOH and filtered through a 0.22 µm filter. The formulation was intravenously administrated to mice via the tail vein (32.5 mg Fe/kg). At various time points, animals were euthanized with Pentoject™ (pentobarbitone sodium 20% w/v, 150 mg/kg) administered via intraperitoneal injection. Blood was immediately collected via cardiac puncture and collected into microtainer tubes coated in EDTA (K2E Vacutainer, BD Biosciences, UK). Various tissues were collected (liver, spleen, brain, heart, lungs and kidneys), thoroughly rinsed in 0.9% w/v NaCl (50 ml) and then stored at -80°C until further analyses could be performed. The tissues were lyophilized, the dry weight was determined and a yttrium standard for ICP was added (1000 ppm, 50 µl, TraceCERT). Dry tissue samples were degraded in $HNO_3$ (70%, 250 µl) for 1 h at 70°C. This was followed by the addition of $H_2O_2$ (30% v/v, 200 µl) and the sample further degraded for 1 h at 70°C. The digestant was cooled, diluted 35-times with MilliQ water and centrifugation (4032 rcf, 10 min) was used to remove any fatty residue. Samples were analyzed using ICP-AES. The iron concentrations were determined based on a calibration curve made from an iron standard for ICP-AES (TraceCERT, Fluka, UK).

### *In vivo* MRI measurements

Female BALB/c mice were used (20–25 g, Harlan). Raspberry SPIONs (5 mg Fe/kg) were administered via the tail vein and images were collected pre-treatment and 1 h post administration of the contrast agent. A multi-slice spin-echo pulse sequence with the following parameters was used to collect axial and coronal images: TE = 6–100 ms, TR = 1845 ms. Animals were anesthetized using isoflurane while the animal's temperature was controlled via a heated bed and its respiration was monitored. All experiments were nonrecovery and animals were euthanized via an overdose of isoflurane and death was confirmed via neck dislocation. The $r_2$ relaxation was determined by curve fitting the echo times (TE) of each pixel in the image using MATLAB (Mathworks, UK). Commercially available Ferucarbotran (Resovist®) was also administrated and measured under the same conditions.

## Results

### Nanoparticle synthesis & morphology

Uniform magnetic nanocrystals were synthesized via high temperature thermal decomposition of an iron–oleate complex in the presence of oleic acid, oleyl alcohol and diphenyl ether, using a method reported by Kim *et al.* [33]. Diphenyl ether was the most suitable high-temperature solvent tested (b.p. 258°C) as the nanoparticles were easily purified, when using this solvent, by washing with acetone. Transmission electron microscopy (TEM) experiments confirmed the presence of nanoparticles, which had an average diameter of 4.8 ± 0.8 nm, were spherical in nature (Figure 1A & B) and could easily be dispersed in hexane, chloroform and tetrahydrofuran (THF). The prepared nanoparticles were coated in a layer of oleic acid, making them extremely hydrophobic and not suitable for biological applications. Nevertheless their hydrophobic surface made them ideal for clustering into raspberry SPIONs as they could be aggregated within an amphiphilic polymer nanoparticle, with the hydrophobic SPION surfaces interacting with the hydrophobic parts of the amphiphilic polymer. The amphiphilic polymer, *N*-palmitoyl-*N*-monomethyl-*N*-*N*-dimethyl-*N*-*N*-*N*-trimethyl-6-O-glycolchitosan (GCPQ), was used to achieve the clustering. The amphiphilic nature of GCPQ allows the polymer to self-assemble into nano-sized micelles of around 32 nm in diameter that are stable even at low polymer concentrations (Supplementary Figure 1) [18]. The hydrophobic oleic acid coated SPIONs may be incorporated into GCPQ nanoparticles by a system of emulsification, with the aid of ultrasonication, followed by organic solvent evaporation. This method yielded raspberry SPIONs (Figure 1C–F) with the hydrophobic oleic acid coated SPIONs located within the core of the polymer nanoparticle (Figure 1D &


10.2217/nnm-2018-0370

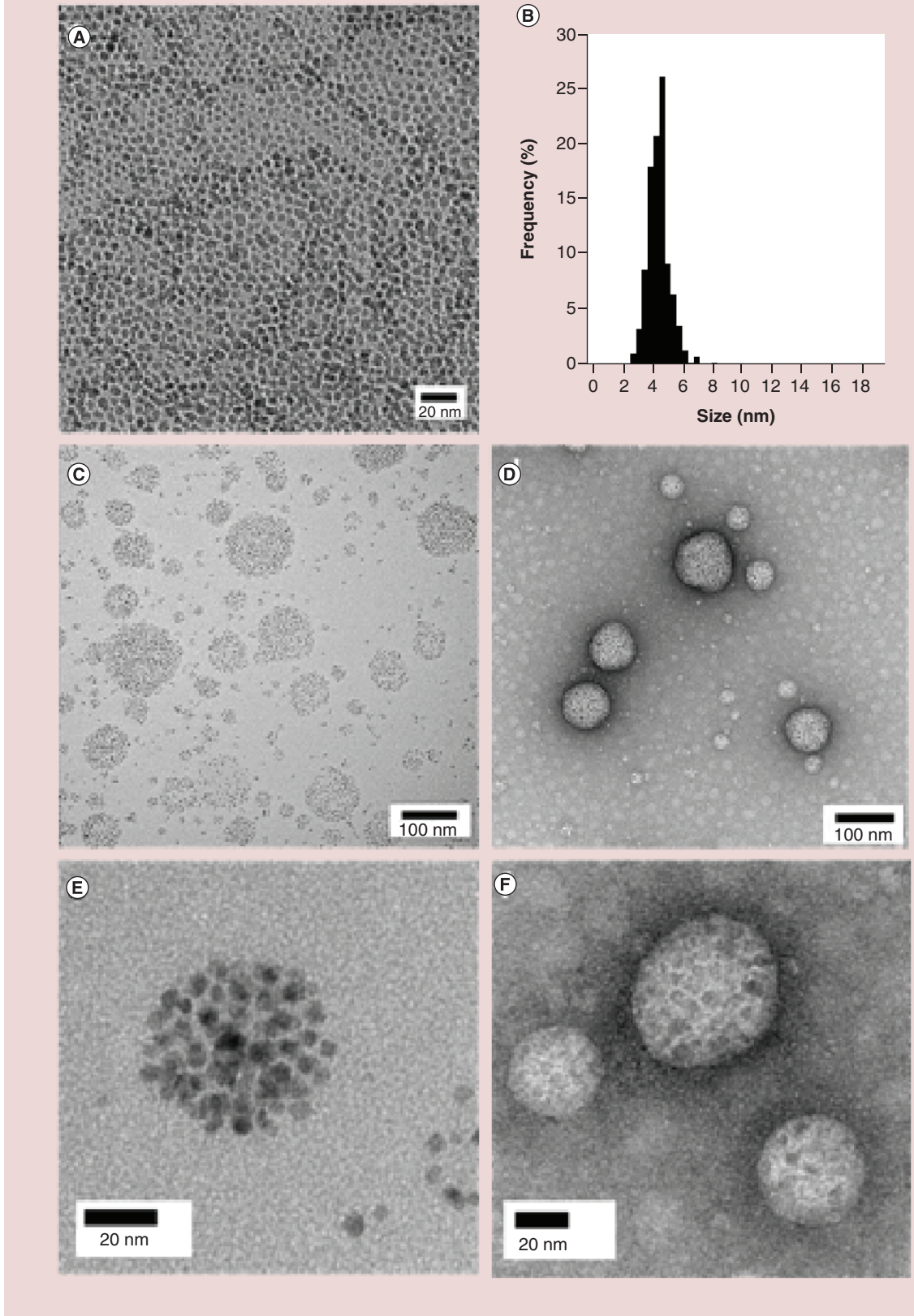


**Figure 1. Transmission electron microscopy images of superparamagnetic iron oxide nanoparticles.** Transmission electron microscopy (TEM) image, without staining of the superparamagnetic iron oxide nanoparticles (SPIONs), **(B)** size distribution of SPIONs, mean size ± SD = 4.8 ± 0.8 nm (n > 300), **(C, E)** TEM images, without staining, of SPIONs encapsulated within a polymeric micelle (GCPQ) forming raspberry SPIONS; **(D, F)** TEM images, with uranyl acetate (1%) staining, of raspberry SPIONs.

1F), as evidenced by the white interior spaces and dark coronas surrounding the raspberry SPIONs in the uranyl acetate stained TEM images. The uranyl acetate stain adheres to hydrophilic regions and avoids hydrophobic regions, making the hydrophilic regions black and hydrophobic regions white in the image. FTIR data also shows vibrations for the oleic acid (2924 $cm^{-1}$ = $CH_2$ alkyl stretch) and GCPQ moieties (1647 $cm^{-1}$ = C=O stretch amide and 1059 $cm^{-1}$ = C-O stretch sugar moiety) in the raspberry SPIONs (Supplementary Figure 3). TGA data reveal the removal of both GCPQ and oleic acid from the raspberry SPIONs on heating (Supplementary Figure 4).

## Nanoparticle size & stability

Several raspberry SPION formulations, containing different SPION, GCPQ weight ratios (1:2.5, 1:0.5 and 1:0.25) were formulated in water and sized by dynamic light scattering (DLS) over 90 days. Formulations made with a higher SPION, GCPQ ratio than 1:0.25 did not produce raspberry SPIONs, indicating that a minimum concentration of GCPQ is needed for raspberry SPIONs to form. Raspberry SPIONs, prepared from SPION, GCPQ weight ratios of 1:2.5, 1:0.5 and 1:0.25 have mean diameters (and polydispersity indices in parenthesis) of 140 nm (0.15), 190 nm (0.14) and 230 nm (0.14), respectively (Supplementary Figure 5). These sizes remain relatively unchanged throughout the 90-day period, indicating that the raspberry SPIONs exhibit good colloidal stability and it appears that the raspberry SPION particle size may be controlled by varying the SPION, polymer weight ratio (Figure 2A). It is worth mentioning that some nanoparticles did settle when the formulations were stored for prolonged periods of time (>4 weeks). These raspberry SPIONs are quite dense since they contain a high atomic number element. However, any sediment could be easily re-dispersed with gentle agitation and this sedimentation had no effect on the measured nanoparticle size. A similar phenomenon was also observed by Lin *et al.* with their chitosan SPION [35]. Colloidal stability was also monitored in various liquids of biomedical relevance (water, [PBS, pH = 7.4], 5% w/v dextrose, 0.9% w/v NaCl) at 37°C and raspberry SPION dispersions in these liquids were analyzed after centrifugation, to remove the noncolloidal fraction of the formulation. Analysis involved the measurement of the total iron content in the formulations using the 1,10-phenanthroline iron quantification assay. The raspberry SPIONs retain their colloidal stability over the 48-h period in all the media studied (Figure 2B). The stability of the raspberry SPIONs was also investigated in 50% rat plasma using inductively coupled plasma-atomic emission spectroscopy (ICP-AES) as the 1,10-phenanthroline iron quantification assay did not work with biological samples (Figure 2C). The raspberry SPIONs had satisfactory colloidal stability properties in plasma, retaining 70% of the iron content within the colloidal fraction after 24 h and 66% over 48 h.

## Nanoparticle characteristics

The surface chemistry of a nanoparticle system is an important feature, as it is this solid–liquid interface, which will interact with the environment and influence colloidal stability [36–38] and *in vivo* performance. To investigate the raspberry SPION's surface charge, the zeta potential was measured as a function of pH (Figure 3A). It was found that, like many other nanoparticles of this nature, the zeta potential of the raspberry SPIONs was dependent on pH and that at neutral pH (pH = 7.0) raspberry SPIONs had a positive surface charge (+24.4 ± 1.5 mV). The effect of pH on nanoparticle size was also measured (Figure 3B). It was found that the size of the raspberry SPIONs increased at basic pH (pH > 9), indicating that the raspberry SPIONs aggregate at basic pH. The solubility of GCPQ is reduced at basic pH [39] and this would reduce the hydrophilic head group area of the polymer and in turn the raspberry SPIONs' surface coverage by the polymer, resulting, ultimately in aggregation.

x-ray diffraction (XRD) patterns were collected on the raspberry SPIONs and the oleic acid coated SPIONs (Figure 3C). The diffraction patterns are similar to the patterns previously reported for SPIONs made via high-temperature thermal decomposition [40–42]. One noticeable characteristic observed was that diffraction peaks obtained were weak in intensity and broad in nature and this is due to the small nanoparticle crystal size. The average crystal size of the oleic acid SPIONs determined by the XRD data and calculated by the Scherrer equation was (3.6 ± 0.1) nm. The small decrease in measured size from that found using the TEM images could be due to the spin canting effect, a small, noncrystalline layer often found on the surface of SPIONs [43], which would be unaccounted for in the XRD assay.

The magnetic behavior of the raspberry SPIONs was investigated by collecting field-dependant magnetization plots (M vs H plots) using a super quantum interference device (SQUID) (Figure 3D). Both the oleic acid coated SPIONs and the raspberry SPIONs display superparamagnetic behavior with no observable remnant magnetization. The magnetic saturation of the oleic acid coated SPIONs and raspberry SPIONs was found to be 29.6 ± 3.7 emu/g Fe and 33.8 ± 1.8 emu/g Fe, respectively. The raspberry SPIONs do exhibit a small increase in

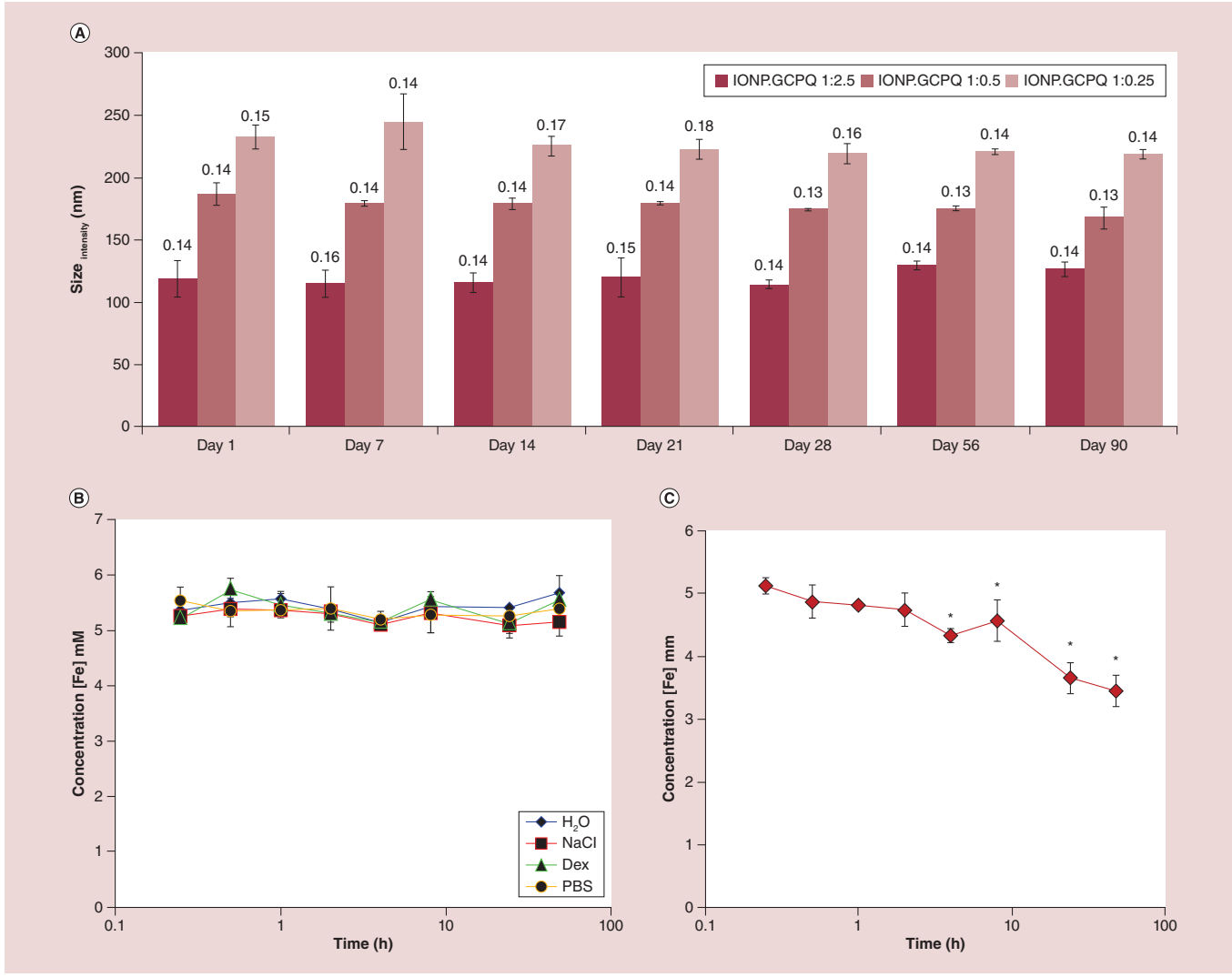


**Figure 2. Superparamagnetic iron oxide nanoparticle stability.** Raspberry superparamagnetic iron oxide nanoparticle (SPION) colloidal stability was investigated by DLS in water over 90 day at 5°C. Polydispersity values were given in labels above each column. No significant difference to the formulation on day 1 was observed in any of the formulations studied over the time period, suggesting that the raspberry SPIONs are colloidally stable in aqueous conditions. Data are means ± SD, n = 3 ($p > 0.05$, one-way ANOVA, Games-Howell post hoc test). **(B)** Raspberry SPION colloidal stability was investigated in various biomedically relevant liquids at 37°C ($H_2O$, PBS, 5% w/v dextrose, 0.9% w/v NaCl). The iron concentration was monitored using the 1,10-iron phenanthroline assay. No significant differences in iron content, over the time period, were observed in any of the media tested suggesting that the raspberry SPIONs were stable in these media over the time period. Data are means ± SD, n = 3 ($p > 0.05$, one-way ANOVA, Tukey post hoc test). **(C)** Raspberry SPION stability was investigated in 50% rat plasma at 37°C. The iron concentration was monitored using ICP-AES. A statistically significant change in iron content was observed over the time period indicating a slight nanoparticle instability in plasma; however, colloidal stability was satisfactory as 70% of the iron content was retained over 24 h. Results suggest that while the raspberry SPIONs change slightly on incubation in plasma, their stability is satisfactory for their imaging application. Data are means ± SD; n = 3 ($p < 0.05$, one-way ANOVA, Tukey post hoc test).

magnetic saturation, when compared with the oleic acid coated SPIONs; however, this result was not statistically significant (p-value > 0.05), suggesting that encapsulation within the polymer nanoparticles has little effect on the magnetic behavior of the SPIONs.

To investigate the MRI contrast behavior of the raspberry SPIONs, their spin-lattice relaxation ($r_1$) and their spin-spin relaxation ($r_2$) were measured as a function of iron concentration using a 1T bench-top MRI scanner (ICON; Figure 3E). The raspberry SPIONs produced an $r_1$ value of 0.66 $mM^{-1}$ $s^{-1}$ and an $r_2$ value of 51.8 $mM^{-1}$ $s^{-1}$, giving an $r_2/r_1$ of 79.1. This high $r_2/r_1$ value for SPIONs with a core size of 5 nm, indicates that a highly effective negative contrast agent has potentially been created [44,45].

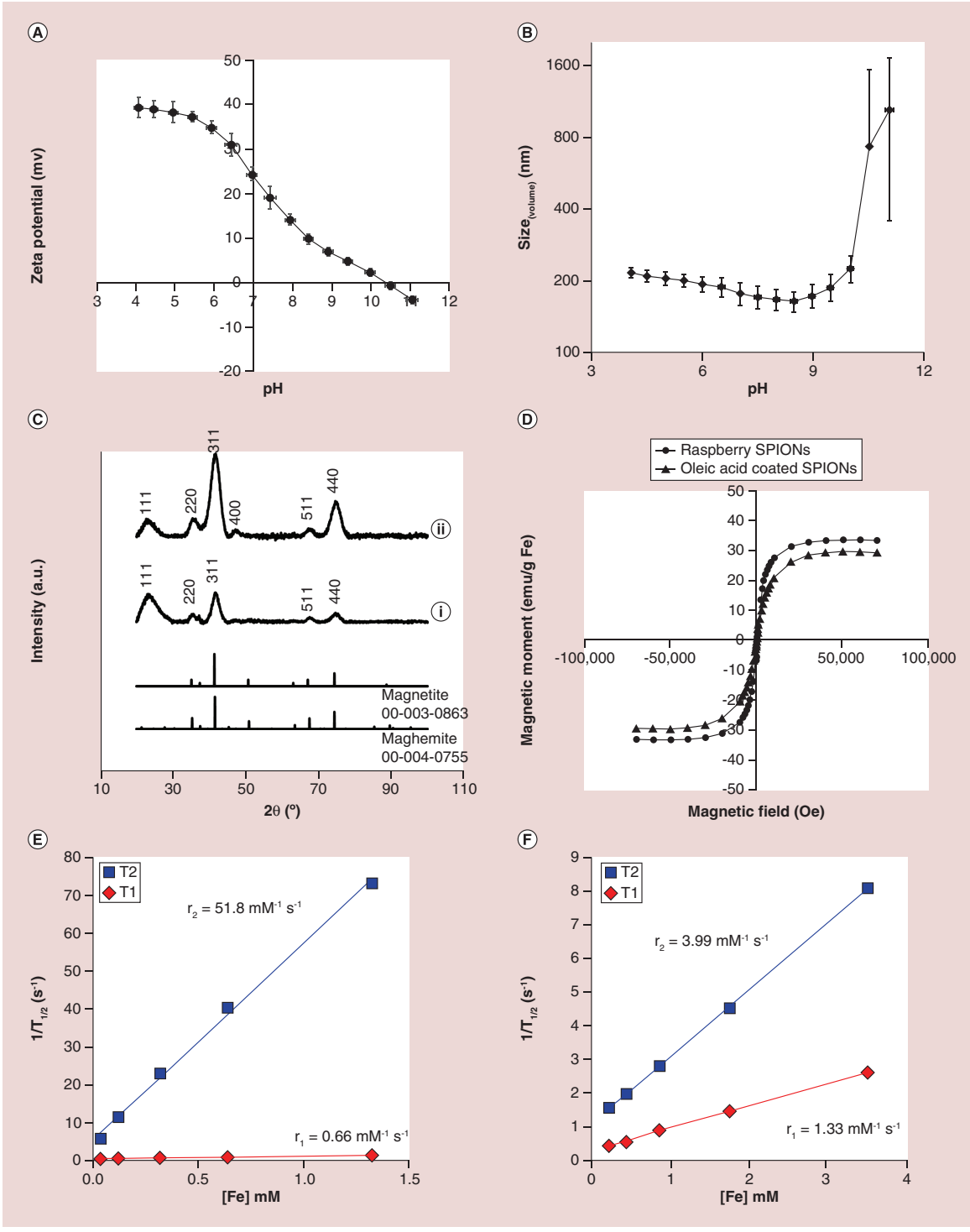


**Figure 3. Characterisation of superparamagnetic iron oxide nanoparticles. (A)** Zeta potential titration to study the effect of pH on raspberry SPION surface charge. Raspberry SPIONs have a positive (+24.4 ± 1.5 mV) zeta potential at neutral pH (pH 7.0). Data are means ± SD n = 3; **(B)** Dynamic light scattering titration to study the effect of pH on nanoparticle size. In strongly basic conditions (pH > 9), aggregation is observed with the raspberry SPIONs, a strong indicator of colloidal instability at alkaline pH. Data are means ± SD n = 3; **(C)** x-ray diffraction patterns of the **(i)** raspberry SPIONs and **(ii)** oleic acid coated SPIONs (5 nm). Both patterns indicate the presence of magnetic iron oxide. **(D)** M versus H plot at 300 °K comparing the magnetic iron content of the raspberry SPIONs and the oleic acid coated SPIONs. Samples of oleic acid coated SPIONs and raspberry SPIONs were measured for iron content and then plotted against their magnetization profile. This yielded a magnetic saturation value of (29.6 ± 3.7) emu/g Fe and (33.8 ± 1.8) emu/g Fe for the oleic acid coated SPIONs and raspberry SPIONs, respectively. There is no significant change in magnetization between the two curves, showing that the clustering of SPIONs has little to no effect on the SPION's magnetization. Data are means ± SD n = 3 ($p < 0.05$, Student's t-test); **(E)** Plot of $1/T_1$ ($s^{-1}$) and $1/T_2$ ($s^{-1}$) against the concentration of Fe in raspberry SPIONs; **(F)** Plot of $1/T_1$ ($s^{-1}$) and $1/T_2$ ($s^{-1}$) against the concentration of Fe in dimercaptosuccinic acid SPIONs (mM). The relaxivities ($r_1$ and $r_2$) can be determined from the slope of the plots. SPION: Superparamagnetic iron oxide nanoparticle.

To investigate the effect of clustering the SPIONs within polymer nanoparticles, the relaxivity of a single crystal (nonclustered) SPION dispersion was measured. The single crystal SPION was achieved by coating the surface of the oleic acid coated SPIONs with DMSA using the ligand exchange procedure outlined by Palma *et al.* [34]. The DMSA SPIONs were colloidally stable in aqueous conditions and had an average hydrodynamic diameter of 9 nm (Supplementary Figure 6). The relaxivity values of the DMSA SPIONs were $r_1$ = 1.33 $\mu M^{-1}$ $s^{-1}$ and $r_2$ = 3.99 $\mu M^{-1}$ $s^{-1}$, giving an $r_2/r_1$ value of 3.0 (Figure 3F). This large reduction in the $r_2/r_1$ value suggests that the DMSA SPIONs are a much weaker negative contrast agent and possibly a more favorable positive contrast agent [33,45]. The data suggest that encapsulating the SPIONs within GCPQ nanoparticles, reduces their spin-lattice relaxation and increases their spin-spin relaxation.

## Nanoparticle *in vivo* pharmacokinetics

To determine the *in vivo* biodistribution of the raspberry SPIONs, the raspberry SPIONs were injected intravenously (32.5 mg Fe/kg), tissues (blood, liver, spleen, brain, lungs, kidney and heart) were collected at various time points and the iron content was measured using ICP-AES. A relatively large dose was administered in order to distinguish SPION iron levels from the endogenous iron levels found in the blood and organs. Blood samples showed a sharp increase in iron concentration over background levels and by the first 15 min time point, 61% of the injected dose was present in the blood (Figure 4A). After this point, the iron concentration continued to decay and by the 1-h time point 43% of the injected dose was present in the blood and iron concentration in the blood had reached background levels by the 8-h time point. The raspberry SPIONs have a blood half-life ($t_{1/2}$) of 28.3 min. Our data show that the raspberry SPIONs accumulate in the liver and spleen (Figure 4B & C). By the first 15-min time point, 23% of the injected dose is present in the liver and 11% of the injected dose is present in the spleen. By the 1-h time point, this increases to 41% in the liver and 15% in the spleen. There was no increase in iron concentration in the brain (Figure 4D), due presumably to the blood–brain barrier, a naturally occurring defence system which is able to exclude foreign particles from entering the brain [46]. A considerable iron increase was detected in the lungs; however, this was cleared after 4 h. The heart and kidneys also exhibited an increase in iron concentration in the early time points (Figure 4F & G). No adverse effects were observed in any of the animals in this experiment, even, when the administered dose was several fold higher than that needed for MRI.

## *In vivo* MRI studies

To evaluate the imaging potential of the raspberry SPIONs *in vivo*, MRI was conducted using a 1T bench-top MRI scanner (ICON). Raspberry SPIONs (5 mg Fe/kg) were injected into the tail vein of female BALB/c mice. A dose of 5 mg Fe/kg has been reported by others previously [47,48]. Pre-treatment and 1 h after injection T2 maps were collected (Figure 5A & B). Noticeable hypointense contrast was observed in the liver parenchyma, to the extent that hepatic liver vessels became noticeably highlighted from the surrounding tissue, showing extravasation of the particles from the liver vasculature. The portal vein also was clearly visible in post contrast images. The benefit of having high levels of contrast in the liver region is that many of the surrounding organs became easy to identify, most notably the kidneys, which were often hard to distinguish from the liver in the pre-treatment images. Negative contrast was also observed in the spleen. The data (Figure 5) correlate well with the pharmacokinetics data (Figure 4), with most of the image darkening being observed in the liver and spleen (Supplementary Figure 8). To assess the raspberry SPIONs' potential clinical relevance, a commercially available SPION negative contrast agent (Ferucarbotran®) was also tested (Figure 5C). As predicted, darkening of the liver was also observed, however many of the fine hepatic liver vessels observed with the raspberry SPIONs were not seen with Ferucarbotran.

To be able to quantify the effect that the raspberry SPIONs had on the T2 relaxivity of the various tissues, T2 relaxivity maps were collected and compared with experiments using no contrast and Ferucarbotran (Supplementary Figure 9). Maps were collected 1 h post administration of the contrast agent. The T2 relaxation was determined by curve fitting the echo times (TE) of each pixel in the image using MATLAB (Mathworks, UK). A summary of the T2 relaxation times of specific regions of interest (lungs, liver, kidneys and spleen) can be seen in Figure 6. The heart could not be mapped accurately as it gave large variations in the data collected. This was attributed to movement from the beating heart during the experiment and the data taking several seconds to acquire for each slice. Respiration was accounted for by gating the experimental procedure and the raspberry SPIONs had no significant effect on relaxation time in the lungs unlike Ferucarbotran, which did display a significant effect on relaxation time in the lungs. The same observation was made in the kidneys, with no change in relaxation times seen with the raspberry SPIONs. Both the raspberry SPIONs and Ferucarbotran produced significant effects

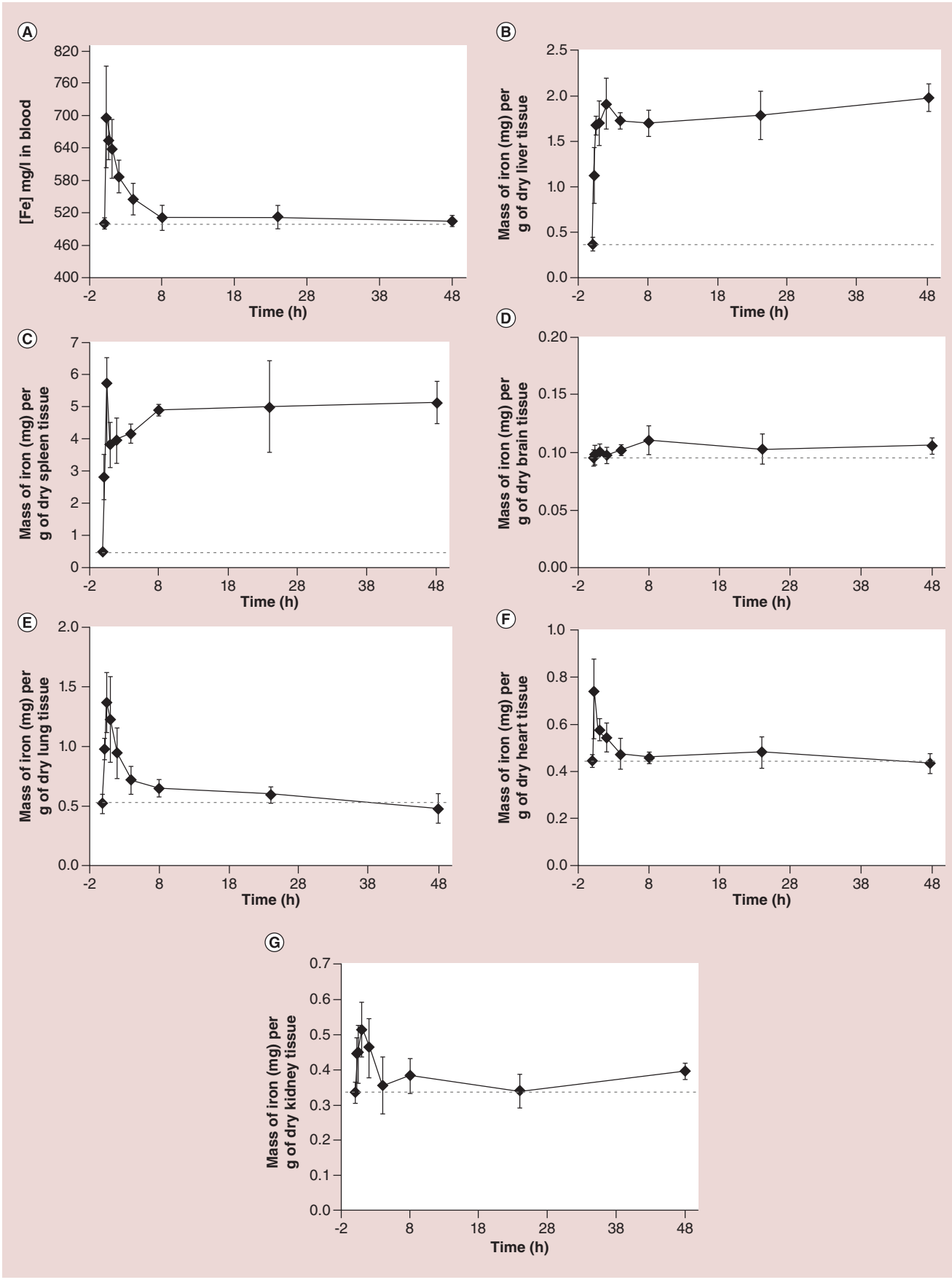


**Figure 4. Iron concentrations (mean ± SD; n = 5) were monitored in various tissues using ICP-AES following tail vein injection into female BALB/c mice. (A)** blood; **(B)** liver; **(C)** spleen; **(D)** brain; **(E)** lung; **(F)** heart; **(G)** kidney. Injected dose was 32.5 mg Fe/kg.

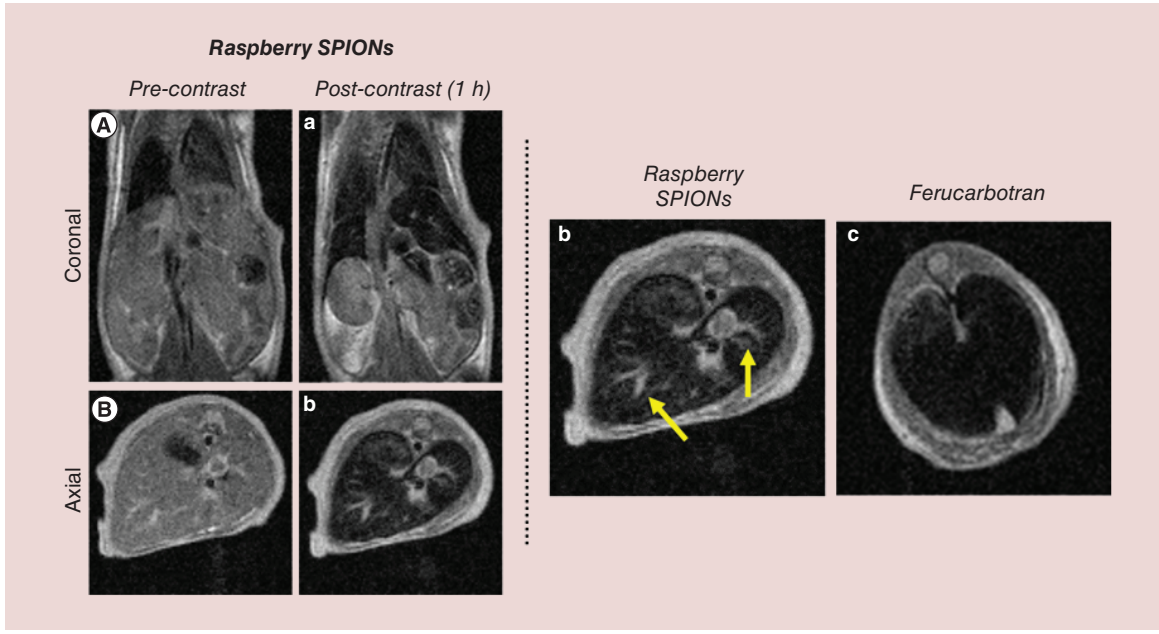


**Figure 5. MRI imaging with SPIONs.** T2 weighted MRI images using the raspberry SPIONs (TE 20 ms) (left); Images **(A & B)** taken pre-administration of the contrast agent and images **(a & b)** taken 1 h after the administration of the contrast agent (right). A comparison of the T2 weighted axial MRI images of a liver cross section 1 h after using: **(B)**, the raspberry SPIONs and **(C)**, the commercially available Ferucarbotran®. Both contrast agents display considerable darkening of the liver; however, hepatic liver vessels can clearly be seen in the post contrast images using the raspberry nanoparticles (arrowed) which were not seen using the commercially available product (n = 1).

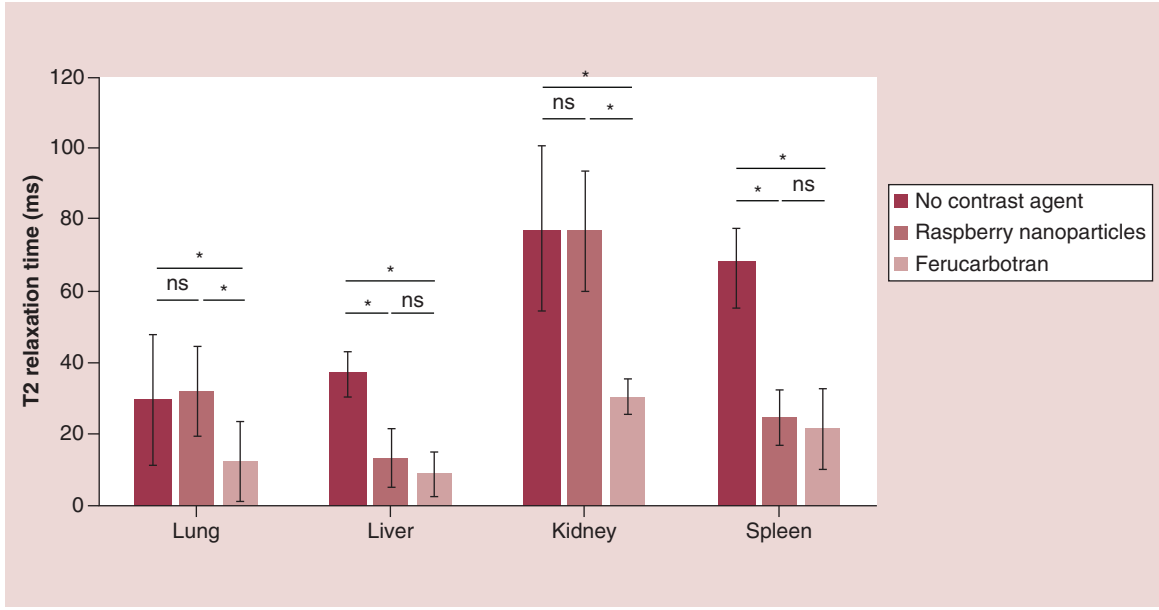


**Figure 6. A summary of the effect on T2 relaxation times in various organs when using the raspberry SPIONs compared with no contrast agent and the commercially available product Ferucarbotran®, all dosed at 5 mg kg$^{-1}$.** Maps were collected 1 h post administration with the contrast agents. The heart was unable to be mapped most likely due to movement from the beating heart during the experiment. Respiration was accounted for by gating the experimental procedure and as a result, the data show that the raspberry SPIONs had no significant effect on T2 relaxation in the lungs unlike Ferucarbotran, which did display significant T2 relaxation reduction in the lung. The same observation was made in the kidneys. Both the raspberry SPIONs and Ferucarbotran produced significant signal reduction in the liver and spleen and to a similar extent. Data are means of pixels of interest ± SD (n > 30, significance = $p < 0.05$, 1-way ANOVA, Games–Howell post hoc test).

on relaxivity in the liver and spleen and to a similar extent. Overall, these data show a difference between the raspberry SPIONs and the commercially available Ferucarbotran; at the 1-h time point both species may be used to give hypointense MRI contrast in healthy liver and spleen tissue; however, the raspberry SPIONs do not affect other organs such as the lungs and kidneys making them selective in their organ imaging. In particular, the unique properties of the raspberry SPION, give far superior resolution of the structural features of the liver, such as the liver vasculature, when compared with the commercial product.

## Discussion

We present here raspberry SPIONs which have been prepared by encapsulating oleic acid coated SPIONs within a chitosan amphiphile: GCPQ (Figure 1). The driving force behind this clustering is thought to be due to the removal of the energetic penalty at the oleic acid–water interface, where the water molecules are at an entropy deficit due to their inability to hydrogen bond in all directions and thus is similar to the driving force behind most aqueous self-assemblies [49]. The entropy gain of the water molecules, achieved once the hydrophobic oleic acid coated SPIONs are encapsulated, drives the self-assembly. The eventual result is that the hydrophilic face of the polymer is in contact with the aqueous disperse phase and the hydrophobic portions of the polymer and the oleic acid coated SPIONs are removed from the aqueous phase and buried within the nanoparticle. Others have reported clustering with polymer amphiphiles [50] and low molecular weight amphiphiles [51] and the novelty of the current work lies with the superior MRI contrast images obtained with the clustered SPIONs (Figure 5). The raspberry SPIONs are remarkably stable with no significant change in their colloidal properties for up to 90 days (Figure 2) and exhibited satisfactory stability in plasma, despite the slight loss of iron recorded over the 24-h period. It is known that a protein coating forms on nanoparticles when in contact with plasma [52] and this protein coating may be implicated in the slight drop in iron concentrations observed. Examining all of the stability data we conclude that the raspberry SPIONs are ideal for the imaging application for which they were intended [36,53] and we proceeded to test them.

The raspberry SPIONs produced an $r_1$ value of 0.66 $mM^{-1}$ $s^{-1}$ and an $r_2$ value of 51.8 $mM^{-1}$ $s^{-1}$, giving an $r_2/r_1$ of 79.1. This high $r_2/r_1$ value for SPIONs with a core size of 5 nm, indicates that a highly effective negative contrast agent has potentially been created [44,45]. Others have reported higher $r_2$ values of 128 $mM^{-1}$ $s^{-1}$ on a 0.5 T instrument with SPIONs of 18 nm in diameter; SPIONs that are over three-times the diameter of the current SPIONs [54]. The relatively large SPIONs reported by Yang and colleagues had $r_1$ values of 19 $mM^{-1}$ $s^{-1}$, with a corresponding $r_2/r_1$ value of 6.6, making them likely to be less efficient contrast agents than the current SPIONs. The relaxivity values of the nonclustered DMSA SPIONs were $r_1$ = 1.33 $\mu M^{-1}$ $s^{-1}$ and $r_2$ = 3.99 $\mu M^{-1}$ $s^{-1}$, giving an $r_2/r_1$ value of 3.0 (Figure 3F). This large reduction in the $r_2/r_1$ value suggests that the DMSA SPIONs are a much weaker negative contrast agent [33,45].

The data suggest that encapsulating the SPIONs within GCPQ nanoparticles reduces their spin-lattice relaxation and increases their spin-spin relaxation. These observations can be explained as follows: particles encapsulated within the polymeric nanoparticle undergo the clustering effect, a well-documented phenomenon in which large clusters of packed SPIONs are much more effective at generating magnetic field inhomogeneities and therefore, increase the spin-spin relaxation of the neighboring water protons [26,55,56]. The SPION's ability to affect the spin-lattice relaxation is a less well understood mechanism, although a compelling hypothesis is that encapsulation within the hydrophobic core of the polymer nanoparticle, inhibits the water molecule's dipolar interactions with the magnetic iron cores, a key interaction underpinning the mechanism of spin-lattice relaxation, with the overall result of reducing the spin-lattice relaxation [57,58]. Our data show that encapsulation of SPIONs within polymeric nanoparticles enhances the SPIONs ability to act as potential negative contrast agents.

In order to evaluate these raspberry SPIONs as imaging agents, we examined their biodistribution (Figure 4). The raspberry SPIONs have a blood half-life ($t_{1/2}$) of 28.3 min. Literature findings report considerably varied SPION blood half-lives, typically ranging from several minutes to several hours [53]. This high variation in SPION half-life is often attributed to the variation in size, charge and surface coating of each SPION system under examination. A comprehensive summary of SPION blood half-lives can be found in a review by Arami *et al.* [53]. Our data show that the raspberry SPIONs accumulate in the liver and spleen (Figure 4B & C). Accumulation in the liver and spleen is a common elimination pathway with SPION systems and is most likely the result of the nanoparticles accumulating in the macrophage-rich tissues of the reticuloendothelial system [53,59–61]. Raspberry SPIONs were also delivered to the lungs; however this was cleared after 4 h. SPIONs have been found in the lungs in other reports and this is often attributed to the lung's large vasculature combined with the presence of macrophage-rich

tissue in the alveoli (Figure 4E) [62,63]. In this case, it appears as if the SPIONs present in the blood pool in the lungs are responsible for the lung iron levels seen. It is also possible that the limited lung tissue accumulation could have been due to the short plasma half-life of the SPIONs. The heart and kidneys also exhibited an increase in iron concentration in the early time points and this is probably also due to the raspberry SPIONs present in the blood pool (Figure 4F & G). It is likely that the iron found in the lung, heart and kidney is due to the blood pool in these organs as the decay kinetics mirror the blood decay kinetics. Ultimately the value of these raspberry SPIONs resides in their ability to be used for MRI imaging. From the findings presented here, this novel contrast agent could be used with shorter MRI scan times to image whole body pathological conditions whereas at longer scan times, it could be used for imaging organs of the reticuloendothelial system such as the liver and spleen.

On intravenous administration of the raspberry SPIONs, noticeable hypointense contrast was observed in the liver parenchyma, to the extent that hepatic liver vessels became noticeably highlighted from the surrounding tissue, showing extravasation of the particles from the liver vasculature. The portal vein also was clearly visible in post contrast images. Negative contrast was also observed in the spleen. The data (Figure 5) correlate well with the pharmacokinetics data (Figure 4) and the T2 relaxation data (Figure 6), with most of the image darkening being observed in the liver and spleen (Supplementary Figure 8). The T2 relaxation data with the raspberry SPIONs was localized in the liver and spleen (Figure 6). Whilst with the commercially available SPION negative contrast agent (Ferucarbotran), T2 relaxation was seen in all the organs examined (Figure 6), the raspberry SPIONs target the image contrast to the liver and spleen, making them selective for imaging these organs.

The hepatic liver vessels were not visualised with Ferucarbotran (Figure 5C). The reason why these hepatic liver vessels are visualized with the raspberry SPIONs and not with the commercially available Ferucarbotran is hypothesized to be due predominantly to the surface chemistry and size differences of the nanoparticles under investigation. The raspberry SPIONs and Ferucarbotran have average hydrodynamic sizes of 190 and 50 nm, respectively. After injection into the blood, the smaller sized Ferucarbotran nanoparticles have the ability to pass from the blood to the nonphagocytic liver sinusoidal endothelial cells [64] that line the liver sinusoids; via clathrin-mediated endocytosis or to pass through their many fenestrations (which allow bidirectional flow of solutes and small particles less than 100–150 nm from the blood to the liver parenchyma and vice versa). In contrast, the larger raspberry SPIONs are liable to be phagocytosed by resident liver macrophages located in the luminal side of the lining of the liver sinusoid taking the hypointense contrast away from the lumen of the blood vessels. In essence, clustering enabled an extravascular localization in the liver and a more intense MRI contrast in extravascular region, which enabled imaging of the vasculature. Accumulation of negatively charged 105 nm latex beads has been reported in the liver Kupffer cells by Tanimoto and colleagues [65]. Considerably more darkening was noticed in the lungs when using Ferucarbotran than was observed with the raspberry nanoparticles (Supplementary Figure 8). The reason for this is that the raspberry SPIONs do not accumulate in the lung tissue (Figure 4E & Figure 6).

The unique properties of the raspberry SPIONs, give far superior resolution of the structural features of the liver, such as the liver vasculature, when compared with the commercial product.

## Conclusion

In conclusion, highly crystalline 5 nm SPIONs were synthesized via high temperature thermal decomposition and clustered into raspberry shapes by a polymeric amphiphile using physical means and without the need for cross-linking. These raspberry SPIONs are colloidally stable in a range of biomedical liquids. MRI experiments demonstrate that this clustering of SPIONs greatly enhances the $r_2$ relaxivity and decreases the $r_1$ relaxivity compared with the single crystals alone, giving an effective negative contrast agent. The blood half-life of the raspberry SPIONs is 28.3 min in rodents and the raspberry SPIONs accumulate in the liver and spleen. Finally, *in vivo* MRI studies show that these new raspberry SPIONs act as effective MRI contrast agents in the liver and spleen, localizing in the liver extravascular space and allowing the unique visualization of the liver vasculature, including the portal vein, when compared with commercially available SPIONs.

## Future perspective

It is predicted that the future of medicine will be heavily focused on more effective diagnostics and as such a diagnostic nanoparticle has been created that could be used to better understand liver disease pathology. It is possible that the knowledge gained in this study will inform the development of more efficient contrast agents.

## Summary points

- This work details the preparation of raspberry superparamagnetic iron oxide nanoparticles (SPIONs), a new class of micelle-based MRI T2 contrast agent made using SPIONs and a chitosan amphiphile (GCPQ).
- Raspberry SPIONs have favorable colloidal stabilities in a range of biologically relevant media ($H_2O$, 0.9% NaCl, 5% dextrose, 1× PBS and 50% rat plasma).
- Raspberry SPION size can be controlled (120–230 nm by DLS) by varying the SPION:GCPQ ratio and the raspberry SPIONs are positively charged at neutral pH.
- XRD confirms the presence of magnetic iron oxide and SQUID assays confirm that the raspberry SPIONs are superparamagnetic and that SPION encapsulation does not diminish their magnetic properties.
- Clustering into raspberry SPIONs greatly increases the spin-spin (r2) to spin-lattice (r1) relaxation ratio (r2/r1) from 3.0 to 79.1.
- Raspberry SPIONs have a blood half-life of 28.3 min and specifically accumulated in the liver and spleen.
- Raspberry SPIONs give high T2 contrast to the extravascular space in the liver, yielding especially detailed images of liver vasculature.
- Raspberry SPIONs may thus be used to selectively image the liver and provide a degree of spatial resolution not previously obtained for the liver.

### Author contributions

NJ Hobson was responsible for the design, synthesis, analysis and evaluation of the work reported in the study. X Weng was involved with experimental and analytical design, ICP-AES analysis and helpful discussions. B Siow conducted the MRI experimentation. C Veiga assisted with the processing and evaluation of the MRI data. IF Uchegbu, AG Schätzlein, NTK Thanh and M Ashford conceived, designed and supervised the study. NJ Hobson wrote the first draft of the manuscript.

### Acknowledgments

The authors would like to thank D McCarthy for help with the TEM images and P Southern for his support with the SQUID.

### Financial & competing interests disclosure

The authors thank the UK Engineering and Physical Sciences Research Council for a PhD studentship to NJ Hobson (EP/L01646X/1). This project was supported by AstraZeneca, UK. The authors have no other relevant affiliations or financial involvement with any organization or entity with a financial interest in or financial conflict with the subject matter or materials discussed in the manuscript apart from those disclosed.

No writing assistance was utilized in the production of this manuscript.

### Ethical conduct of research

All animal work was conducted under a UK Home Office Licence and approved by a UCL local ethics committee. The authors state that they have obtained appropriate institutional review board approval or have followed the principles outlined in the Declaration of Helsinki for all human or animal experimental investigations.



## References

Papers of special note have been highlighted as: • of interest

1. Mansfield EA. FDA perspective on companion diagnostics: an evolving paradigm. *Clin. Cancer Res.* 20(6), 1453–1457 (2014).
2. Agarwal A, Ressler D, Snyder G. The current and future state of companion diagnostics. *Pharmacogenics Pers. Med.* 8, 99–110 (2015).
3. McRobbie DW, Moore EA, Graves MJ, Prince MR. *MRI from Picture to Proton* Cambridge University Press, Cambridge (2006).
4. Geraldes CF, Laurent S. Classification and basic properties of contrast agents for magnetic resonance imaging. *Contrast Media. Mol. Imaging* 4(1), 1–23 (2009).
5. Thanh NTK. *Magnetic Nanoparticles: From Fabrication to Clinical Applications* Taylor & Francis, London, UK (2012).

• **A review on the use of magnetic nanoparticles which will introduce the reader to the subject within an appropriate context.**

6. Corot C, Robert P, Idée J-M, Port M. Recent advances in iron oxide nanocrystal technology for medical imaging. *Adv. Drug Deliv. Rev.* 58(14), 1471–1504 (2006).

- **A review on the use of magnetic resonance imaging with iron oxide nanoparticles which introduces many technical aspects of the systems.**

7. Saini S, Stark DD, Hahn PF *et al.* Ferrite particles: a superparamagnetic MR contrast agent for enhanced detection of liver carcinoma. *Radiology* 162(1), 217–222 (1987).
8. Gupta AK, Gupta M. Synthesis and surface engineering of iron oxide nanoparticles for biomedical applications. *Biomaterials* 26(18), 3995–4021 (2005).
9. Rümenapp C, Gleich B, Haase A. Magnetic nanoparticles in magnetic resonance imaging and diagnostics. *Pharm. Res.* 29(5), 1165–1179 (2012).
10. Kiessling F, Mertens ME, Grimm J, Lammers T. Nanoparticles for imaging: top or flop? *Radiology* 273(1), 10–28 (2014).
11. Wang Y-XJ. Superparamagnetic iron oxide based MRI contrast agents: current status of clinical application. *Quant. Imaging Med. Surg.* 1(1), 35–40 (2011).
12. Wang Y-XJ. Current status of superparamagnetic iron oxide contrast agents for liver magnetic resonance imaging. *World J. Gastroenterol.* 21(47), 13400–13402 (2015).
13. European Medicines Agency. Withdrawal Assessment Report for Sinerem (2008). https://www.ema.europa.eu/en/medicines/human/withdrawn-applications/sinerem
14. Tietze R, Alexiou C. Improving cancer imaging with magnetic nanoparticles: where are we now? *Nanomedicine (Lond)* 12(3), 167–170 (2017).
15. Rogosnitzky M, Branch S. Gadolinium-based contrast agent toxicity: a review of known and proposed mechanisms. *Biometals* 29(3), 365–376 (2016).
16. Fisusi FA, Siew A, Chooi KW *et al.* Lomustine nanoparticles enable both bone marrow sparing and high brain drug levels – a strategy for brain cancer treatments. *Pharm. Res.* 33(5), 1289–1303 (2016).

- **An article detailing the use of the chitosan amphiphile on intravenous delivery and for the treatment of experimental tumors.**

17. Lalatsa A, Garrett NL, Ferrarelli T, Moger J, Schätzlein AG, Uchegbu IF. Delivery of peptides to the blood and brain after oral uptake of quaternary ammonium palmitoyl glycol chitosan nanoparticles. *Mol. Pharmaceutics* 9(6), 1764–1774 (2012).
18. Siew A, Le H, Thiovolet M, Gellert P, Schatzlein A, Uchegbu I. Enhanced oral absorption of hydrophobic and hydrophilic drugs using quaternary ammonium palmitoyl glycol chitosan nanoparticles. *Mol. Pharmaceutics* 9(1), 14–28 (2012).
19. Qu X, Khutoryanskiy VV, Stewart A *et al.* Carbohydrate-based micelle clusters which enhance hydrophobic drug bioavailability by up to 1 order of magnitude. *Biomacromolecules* 7(12), 3452–3459 (2006).
20. Godfrey L, Iannitelli A, Garrett NL *et al.* Nanoparticulate peptide delivery exclusively to the brain produces tolerance free analgesia. *J. Control. Release* 270, 135–144 (2017).
21. Uchegbu IF, Sadiq L, Pardakhty A *et al.* Gene transfer with three amphiphilic glycol chitosans - the degree of polymerisation is the main controller of transfection efficiency. *J. Drug Target.* 12(8), 527–539 (2004).

- **A primary paper detailing the biocompatibility assessments of the chitosan amphiphile used in these studies.**

22. Euliss LE, Grancharov SG, O'Brien S *et al.* Cooperative assembly of magnetic nanoparticles and block copolypeptides in aqueous media. *Nano Letters* 3(11), 1489–1493 (2003).
23. Ai H, Flask C, Weinberg B *et al.* Magnetite-loaded polymeric micelles as ultrasensitive magnetic-resonance probes. *Adv. Mater.* 17, 1949–1952 (2005).
24. Cheng D, Hong G, Wang W *et al.* Nonclustered magnetite nanoparticle encapsulated biodegradable polymeric micelles with enhanced properties for in vivo tumor imaging. *J. Mater. Chem.* 21(13), 4796–4804 (2011).
25. Lee HJ, Jang K-S, Jang S *et al.* Poly(amino acid)s micelle-mediated assembly of magnetite nanoparticles for ultra-sensitive long-term MR imaging of tumors. *Chem. Commun.* 46(20), 3559–3561 (2010).
26. Guang Choo ES, Tang X, Sheng Y, Shuter B, Xue J. Controlled loading of superparamagnetic nanoparticles in fluorescent nanogels as effective T2-weighted MRI contrast agents. *J. Mater. Chem.* 21(7), 2310–2319 (2011).
27. Li X, Li H, Liu G *et al.* Magnetite-loaded fluorine-containing polymeric micelles for magnetic resonance imaging and drug delivery. *Biomaterials* 33(10), 3013–3024 (2012).
28. Pöselt E, Kloust H, Tromsdorf U *et al.* Relaxivity optimization of a PEGylated iron-oxide-based negative magnetic resonance contrast agent for T2-weighted spin–echo imaging. *ACS Nano* 6(2), 1619–1624 (2012).
29. Su H, Liu Y, Wang D *et al.* Amphiphilic starlike dextran wrapped superparamagnetic iron oxide nanoparticle clsuters as effective magnetic resonance imaging probes. *Biomaterials* 34(4), 1193–1203 (2013).
30. Pham BTT, Colvin EK, Pham NTH *et al.* Biodistribution and clearance of stable superparamagnetic maghemite iron oxide nanoparticles in mice following intraperitoneal administration. *Int. J. Mol. Sci.* 19(1), 205 (2018).

31. Wei H, Bruns OT, Kaul MG *et al.* Exceedingly small iron oxide nanoparticles as positive MRI contrast agents. *Proc. Natl Acad. Sci. USA* 114(9), 2325–2330 (2017).
32. Wang W, McConaghy AM, Tetley L, Uchegbu IF. Controls on polymer molecular weight may be used to control the size of palmitoyl glycol chitosan polymeric vesicles. *Langmuir* 17(3), 631–636 (2001).
33. Kim BH, Lee N, Kim H *et al.* Large-scale synthesis of uniform and extremely small-sized iron oxide nanoparticles for high-resolution T1 magnetic resonance imaging contrast agents. *J. Am. Chem. Soc.* 133(32), 12624–12631 (2011).
34. Palma SICJ, Marciello M, Carvalho A, Veintemillas-Verdaguer S, Morales MdP, Roque ACA. Effects of phase transfer ligands on monodisperse iron oxide magnetic nanoparticles. *J. Colloid Interface Sci.* 437, 147–155 (2015).
35. Lin Y, Wang S, Zhang Y *et al.* Ultra-high relaxivity iron oxide nanoparticles confined in polymer nanospheres for tumor MR imaging. *J. Mater. Chem. B* 3(28), 5702–5710 (2015).
36. Moghimi SM, Hunter AC, Murray JC. Long-circulating and target-specific nanoparticles: theory to practice. *Pharmacol. Rev.* 53(2), 283–318 (2001).
37. Mahmoudi M, Sant S, Wang B, Laurent S, Sen T. Superparamagnetic iron oxide nanoparticles (SPIONs): development, surface modification and applications in chemotherapy. *Adv. Drug Del. Rev.* 63(1–2), 24–46 (2011).
38. Pfeiffer C, Rehbock C, Hühn D *et al.* Interaction of colloidal nanoparticles with their local environment: the (ionic) nanoenvironment around nanoparticles is different from bulk and determines the physico-chemical properties of the nanoparticles. *J. Royal Soc. Interface* 11(96), 20130931 (2014).
39. Chooi KW, Simao Carlos MI, Soundararajan R *et al.* Physical characterisation and long-term stability studies on quaternary ammonium palmitoyl glycol chitosan (GCPQ) – a new drug delivery polymer. *J. Pharm. Sci.* 103(8), 2296–2306 (2014).

• **A primary paper that introduces the reader to the chitosan amphiphile.**

40. Park J, An K, Hwang Y *et al.* Ultra-large-scale syntheses of monodisperse nanocrystals. *Nat. Mater.* 3(12), 891–895 (2004).
41. Jun Y-w, Huh Y-M, Choi J-s *et al.* Nanoscale size effect of magnetic nanocrystals and their utilization for cancer diagnosis via magnetic resonance imaging. *J. Am. Chem. Soc.* 127(16), 5732–5733 (2005).
42. Roca AG, Morales MP, O'Grady K, Serna CJ. Structural and magnetic properties of uniform magnetite nanoparticles prepared by high temperature decomposition of organic precursors. *Nanotechnology* 17(11), 2783 (2006).
43. Baaziz W, Pichon BP, Fleutot S *et al.* Magnetic iron oxide nanoparticles: reproducible tuning of the size and nanosized-dependent composition, defects, and spin canting. *J. Phys. Chem. C* 118(7), 3795–3810 (2014).
44. Rohrer M, Bauer H, Mintorovitch J, Requardt M, Weinmann H-J. Comparison of magnetic properties of MRI contrast media solutions at different magnetic field strengths. *Investig. Radiol.* 40(11), 715–724 (2005).
45. Tromsdorf UI, Bruns OT, Salmen SC, Beisiegel U, Weller H. A highly effective, nontoxic T1 MR contrast agent based on ultrasmall PEGylated iron oxide nanoparticles. *Nano Letters* 9(12), 4434–4440 (2009).
46. Chen Y, Liu L. Modern methods for delivery of drugs across the blood–brain barrier. *Adv. Drug Del. Rev.* 64(7), 640–665 (2012).
47. Ruiz A, Hernandez Y, Cabal C *et al.* Biodistribution and pharmacokinetics of uniform magnetite nanoparticles chemically modified with polyethylene glycol. *Nanoscale* 5(23), 11400–11408 (2013).
48. Leal MP, Muñoz-Hernández C, Berry CC, García-Martín ML. *In vivo* pharmacokinetics of T2 contrast agents based on iron oxide nanoparticles: optimization of blood circulation times. *RSC Adv.* 5, 76883–76891 (2015).
49. Tanford C. *The Hydrophobic Effect: Formation of Micelles and Biological Membranes*. John Wiley and Sons, NY, USA (1980).
50. Ai H, Flask C, Weinberg B *et al.* Magnetite-loaded polymeric micelles as ultrasensitive magnetic-resonance probes. *Adv. Mater.* 17(16), 1949–1952 (2005).
51. Qiu PH, Jensen C, Charity N, Towner R, Mao CB. Oil phase evaporation-induced self-assembly of hydrophobic nanoparticles into spherical clusters with controlled surface chemistry in an oil-in-water dispersion and comparison of behaviors of individual and clustered iron oxide nanoparticles. *J. Am. Chem. Soc.* 132(50), 17724–17732 (2010).
52. Salvati A, Pitek AS, Monopoli MP *et al.* Transferrin-functionalized nanoparticles lose their targeting capabilities when a biomolecule corona adsorbs on the surface. *Nat. Nanotechnol.* 8(2), 137–143 (2013).
53. Arami H, Khandhar A, Liggitt D, Krishnan KM. *In vivo* delivery, pharmacokinetics, biodistribution and toxicity of iron oxide nanoparticles. *Chem. Soc. Rev.* 44(23), 8576–8607 (2015).
54. Yang LJ, Ma LC, Xin JY *et al.* Composition tunable manganese ferrite nanoparticles for optimized T-2 contrast ability. *Chem. Mater.* 29(7), 3038–3047 (2017).
55. Larsen BA, Haag MA, Serkova NJ, Shroyer KR, Stoldt CR. Controlled aggregation of superparamagnetic iron oxide nanoparticles for the development of molecular magnetic resonance imaging probes. *Nanotechnology* 19(26), 265102 (2008).
56. Vuong QL, Gillis P, Gossuin Y. Monte Carlo simulation and theory of proton NMR transverse relaxation induced by aggregation of magnetic particles used as MRI contrast agents. *J. Magnet. Res.* 212(1), 139–148 (2011).
57. Senpan A, Caruthers SD, Rhee I *et al.* Conquering the dark side: colloidal iron oxide nanoparticles. *ACS Nano* 3(12), 3917–3926 (2009).

58. Caravan P, Ellison JJ, McMurry TJ, Lauffer RB. Gadolinium(III) chelates as MRI contrast agents: structure, dynamics, and applications. *Chem. Rev.* 99(9), 2293–2352 (1999).
59. Jain TK, Reddy MK, Morales MA, Leslie-Pelecky DL, Labhasetwar V. Biodistribution, clearance, and biocompatibility of iron oxide magnetic nanoparticles in rats. *Mol. Pharmaceutics* 5(2), 316–327 (2008).
60. Wagner SD, Schnorr JD, Pilgrimm HP, Hamm BM, Taupitz MM. Monomer-coated very small superparamagnetic iron oxide particles as contrast medium for magnetic resonance imaging: preclinical *in vivo* characterization. *Investig. Radiol.* 37(4), 167–177 (2002).
61. Gu L, Fang RH, Sailor MJ, Park J-H. In vivo clearance and toxicity of monodisperse iron oxide nanocrystals. *ACS Nano* 6(6), 4947–4954 (2012).
62. Xu H, Cheng L, Wang C, Ma X, Li Y, Liu Z. Polymer encapsulated upconversion nanoparticle/iron oxide nanocomposites for multimodal imaging and magnetic targeted drug delivery. *Biomaterials* 32(35), 9364–9373 (2011).
63. Kievit FM, Stephen ZR, Veiseh O *et al.* Targeting of primary breast cancers and metastases in a transgenic mouse model using rationally designed multifunctional SPIONs. *ACS Nano* 6(3), 2591–2601 (2012).
64. Sorensen KK, Simon-Santamaria J, McCuskey RS, Smedsrod B. Liver sinusoidal endothelial cells. *Compr. Physiol.* 5(4), 1751–1774 (2015).
65. Tanimoto A, Oshio K, Suematsu M, Pouliquen D, Stark DD. Relaxation effects of clustered particles. *J. Magn. Reson. Imaging* 14(1), 72–77 (2001).